J Mater Sci (2013) 48:473–480
DOI 10.1007/s10853-012-6761-z

Hot working behavior of AZ31 and ME21 magnesium alloys

S. Gall · M. Huppmann · H. M. Mayer · S. Müller · W. Reimers

Received: 20 March 2012 / Accepted: 19 June 2012 / Published online: 31 July 2012

Abstract The plastic deformation and recrystallization behavior of the commercial magnesium alloys AZ31 and ME21 were analyzed in a wide temperature range. Using the conventional hyperbolic sine equation the flow stress dependence on temperature and strain rate was modeled. The activation energy for plastic deformation significantly increased with increasing temperature and delivered values above 180 kJmol^{-1} for both alloys in the very high-temperature regime (400–550 °C). At lower temperatures (250–400 °C) the activation energy of the AZ31 alloy was approximately 108 kJmol^{-1} considering the peak stress as well as 120 kJmol^{-1} considering the flow stress at a strain of 0.5. The stress exponent varied in a range between 4.5 and 6.5. During the high-temperature compression tests a partial recrystallized microstructure was formed, which was distinctly different in AZ31 compared to ME21 due to the different onset of dynamic recrystallization (DRX) mechanisms.

S. Gall (✉) · S. Müller
Extrusion Research and Development Center, Chair Metallic Materials, TU Berlin, Gustav-Meyer-Allee 25, Sekr. TIB 4/1-2, 13355 Berlin, Germany
e-mail: s.gall@tu-berlin.de

S. Müller
e-mail: soeren.mueller@tu-berlin.de

S. Gall · M. Huppmann · H. M. Mayer · W. Reimers
Chair Metallic Materials, TU Berlin, Ernst-Reuter-Platz 1, Sekr. BH 18, 10587 Berlin, Germany
e-mail: michael.huppmann@tu-berlin.de

H. M. Mayer
e-mail: hans-michael.mayer@tu-berlin.de

W. Reimers
e-mail: walter.reimers@physik.tu-berlin.de

Introduction

Magnesium and its alloys are continuously of important interest due to their high-specific strength and stiffness. However, the ductility and formability of polycrystalline magnesium are poor due to the hexagonal closed packed (hcp) structure with its limited number of slip systems at room temperature. At room temperature basal slip is the dominant slip system since the critical resolved shear stress (CRSS) for basal slip is approximately 100 times lower than for prismatic and pyramidal slip (e.g., [1]). Since slip delivers only two independent slip systems [2] instead of five independent slips systems according to the von Mises criterion for homogeneous deformation at lower temperatures the deformation is carried by the activation of twinning systems. Even though Meyers et al. [3] reported that the twinning is relatively temperature insensitive, with increasing temperature slip dominated deformation occurs due to activation of non-basal slip systems as a result of rapid decrease of their CRSS (e.g., [4, 5]).

The understanding of the plastic deformation behavior over a wide range of temperature, strain, and strain rate is required before performing expensive industrial-scale experiments. In the meantime cost-effective computer modeling of forming processes is state of the art in industry and science for a great number of applications, but reliable material parameters are required. These parameters should be desirably determined by an inexpensive, but failure-safe experimental set-up.

The thermal viscoplastic behavior of a metallic material during hot deformation can be described by the following constitutive relationship using the hyperbolic sine form (e.g., [6]):

$$\dot{\varepsilon}\exp\left(\frac{Q}{RT}\right) = Z = A(\sinh\alpha\sigma)^n, \quad (1)$$

where Z is the temperature compensated strain rate (well-known as Zener–Hollomon parameter), A and n material constants, α the stress multiplier, ε the strain rate, Q the apparent activation energy, R the gas constant, and T the absolute temperature. According to [6] the hyperbolic sine form, which is preferred to predict the flow stresses in a wide range of temperatures and strain rates. The material parameters in this constitutive relationship may be obtained by performing hot working tests determining the flow stress as a function of strain, strain rate, and temperature. For instance, works of Slooff et al. [7, 8] show that hot compression tests are suited to determine reliable material data even at high strains provided that friction is minimized.

By means of the Zener–Hollomon parameter Eq. 1 relates the steady-state flow with the temperature and strain rate without taking strain into account (e.g., [6, 7]). However, the deformation of magnesium alloys is often not in the steady-state, especially at lower temperatures. Therefore, Slooff et al. [7] incorporates strain into the constitutive equation by making the material constant A strain dependent. McQueen and Ryan [6] suggest the determination of the material parameter using the peak stress, because it typically indicates the onset of DRX. However, that suggestion cannot be generalized since e.g., Al-Samman and Gottstein [9] showed that DRX during high-temperature deformation of AZ31 does not start at the peak stress, but already at lower strains. The onset of DRX is usually associated with the inflection point on the curve obtained by plotting strain hardening as a function of flow stress [10, 11].

During hot working processes different mechanisms of recovery (RV) and DRX arise. Thereby, the nucleation process significantly depends on temperature and strain. Galiyev et al. [12] proposed a microstructural model for correlating the plastic deformation and the recrystallization over a wide temperature range. Thus, high-angle boundaries result from a rearrangement of dislocations at low temperatures. At intermediate temperatures dislocation rearrangement by cross-slip and climb generate low-angle boundaries in the vicinity of original grain boundaries [12, 13]. In the case of high-deformation temperatures, the activation energy of plastic flow reaches the activation energy for volume self-diffusion (value: 135 $kJmol^{-1}$ [14]) resulting in dislocation climb as controlling process. Low-angle boundaries will be formed. While bulging of grain boundaries is the predominant DRX mechanism at low strains, at higher strains the nucleation in slip bands occurs.

The present work delivers a study of the hot formability of the commercial magnesium alloys AZ31 and ME21 by means of compression tests over wide temperature and strain ranges. The cast alloys were tested after homogenization, since this is the initial state for forming processes such as extrusion. By the constitutive relationship the material constants are determined for the peak stress and the steady-state condition. Furthermore, the microstructural evolution during hot compression is especially addressed.

Experimental procedures

For the hot compression tests the two commercial magnesium wrought alloys AZ31 and ME21 were used. The magnesium alloy AZ31 with a chemical composition of 2.9 wt% Al, 0.9 wt% Zn, and 0.3 wt% Mn (Mg balance) was supplied by Otto Fuchs KG; Meinerzhagen (Germany). The ME21 alloy containing 2.1 wt% Mn, 0.7 wt% Ce, and 0.1 wt% Th (Mg balance) was received from Stolfig-Group; Geisenfeld (Germany). Both alloys were manufactured by continuous casting. After the casting the billets were homogenized for 12 h at a temperature of 350 °C (AZ31) and of 400 °C (ME21), respectively.

The alloys were delivered in the form of round billets. Therefore, in each case a disk with an accurate thickness of 15 mm was cut out of each billet. Using wire-electro discharge machining cylindrical compression specimens with dimensions of 15 mm in height and 10 mm in diameter, were finally prepared.

The hot compression tests were carried out with the thermo-mechanical simulator Gleeble Systems 3800 at ambient pressure. For temperature control during the tests a thermocouple was welded onto the surface at mid height. Between the specimen and the tungsten carbide punch a graphite slice (thickness 0.12 mm) with a thin film of nickel-containing paste was applied to reduce the friction. The specimen was resistance-heated at a rate of 5 Ks^{-1} and kept at the preset temperature for 60 s to allow the temperature to equalize. After deformation the specimen was air-cooled to ambient temperature. Since at high-strain rates (1 s^{-1}) the temperature of the specimen was not constant during deformation due to the adiabatic heating, the flow stress data had to be corrected using the method by Goetz and Semiatin [15]. For a comparative study of both magnesium alloys the test temperature was ranged between 400 and 550 °C using steps of 50 K. Furthermore, for the AZ31 alloy compression tests were performed at lower temperature between 200 and 400 °C. The ME21 specimens were not tested in that lower temperature regime, since they showed shear fracture at an early stage of deformation. Huppmann et al. [16] reported same observations for compression specimens machined out of non-homogenized cast billets. For both alloys strain rates of 0.01, 0.1, 1, and 5 s^{-1} were used. Please note that the stresses and the strains using in the figures throughout this publication are given (and were respectively used for calculation) in absolute values, i.e., without negative sign.

The microstructure of the homogenized material and the hot-deformed compression specimen were investigated by optical microscopy. Therefore, the specimens were ground and polished using the automatic grinding and polishing machine TegraPol-25. Grinding was carried out in five steps up to 4,000 grit silicon carbide and polishing was done with 3 µm, 1 µm diamond suspension as well as 0.2 silicon oxide. Afterward, the AZ31 specimens were electropolished and finally etched with picric acid solution containing 5 g picric acid, 6 ml acetic acid, 20 ml H_2O, and 100 ml ethanol. In contrast the ME21 were chemically polished using a CP2 solution containing 12 ml hydrochloric acid (37 %), 8 ml nitric acid (65 %), and 100 ml ethanol and finally etched with picric acid solution composed of 4.2 g picric acid, 10 ml acetic acid, 10 ml H_2O, and 70 ml ethanol.

Results and discussions

After continuous casting and homogenization both magnesium alloys exhibited equiaxed grains with sizes ranging from 0.2 to 5 mm in the microstructure. In the AZ31 material the Al-rich precipitates and Mn-rich particles were homogeneously distributed (Fig. 1a). The grains in the ME21 material exhibited dendritic and non-dendritic microstructures as well as twins (Fig. 1b). As already described in the work of Huppmann et al. [16] $Mg_{12}Ce$ precipitates were found in the microstructure in the form of large elongated precipitates along the grain boundaries as well as in form of ellipsoidal particles in between the dendritic arms. In addition very fine pure manganese precipitates (<100 nm), which exist in the matrix and at the interface between the $Mg_{12}Ce$ precipitates and the Mg matrix were identified.

In Fig. 2 for both alloys selected stress–strain curves performed at test temperatures of 400 and 500 °C are presented. As expected the absolute stress values decrease with decreasing strain rate and increasing temperature, respectively. At the beginning of the deformation the curves increase due to work hardening, resulting in a peak stress at 400 °C and a strain range of 0.1–0.2 for AZ31. After the peak stress the stress–strain curves decrease down to steady-state flow due to softening. The peak shape is more pronounced with increasing strain rate due to the strain rate sensitivity at elevated temperatures [5, 17]. At higher temperatures peak stress occurs only for high-strain rates. Independent from the temperature the ME21 specimens show a gradual increase in the stress–strain curves without sharply formed peak stress. Most curves continuously rise to steady-state flow. The maximum stresses are generally reached in a strain range of 0.4–0.5.

Looking in detail, at the test temperature of 400 °C AZ31 exhibits a more pronounced work hardening than

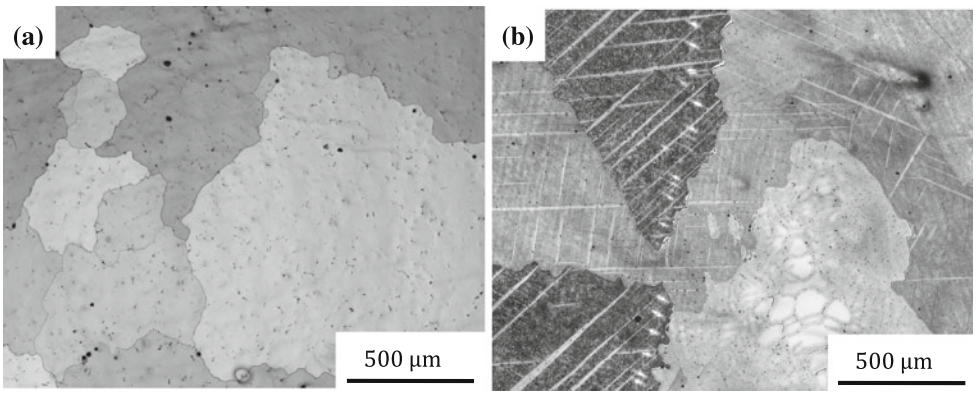

Fig. 1 Structure of the initial material after homogenization: **a** AZ31, **b** ME21

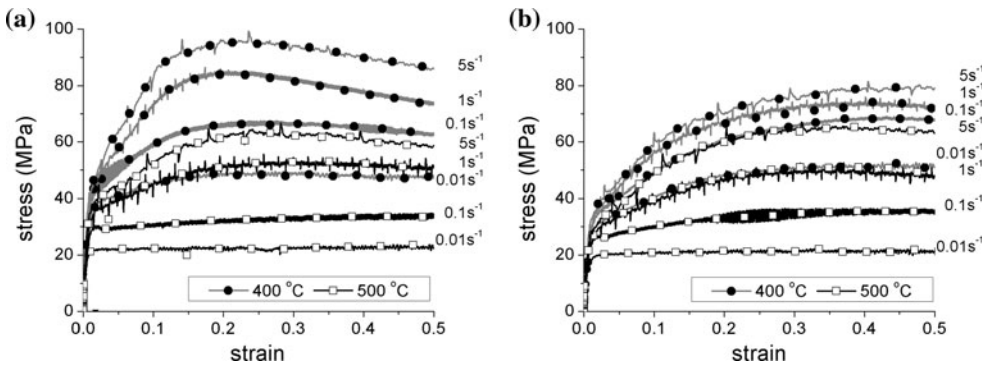

Fig. 2 Selected stress–strain curves up to a strain of 0.5 for different strain rates and temperatures: **a** AZ31, **b** ME21

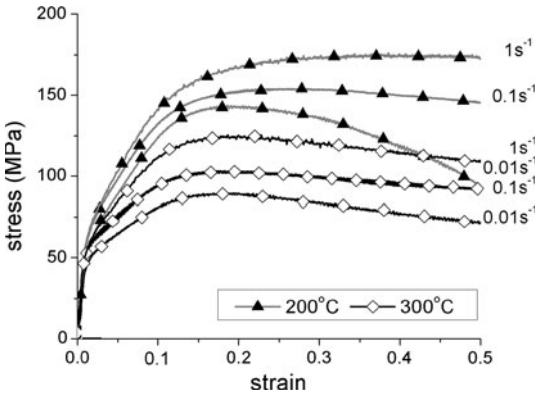

Fig. 3 Selected stress–strain curves up to a strain of 0.5 for AZ31 at test temperatures of 200 and 300 °C

ME21. Furthermore, AZ31 delivers higher stress values for high-strain rates (1, 5 s^{-1}), but for the intermediate and low-strain rates (0.01, 0.1 s^{-1}) the values of flow stress are comparable with ME21. At very high temperatures (500 °C) the flow stresses of both alloys are approximately in the same range.

Compression tests performed at lower temperatures show an increasing work hardening with increasing strain rate and test temperatures beyond the quasi-elastic regime (Fig. 3.). It is interesting to note that the curves determined at 200 °C and 0.1 s^{-1} as well as 1 s^{-1} do not show a pronounced peak. In contrast the curve obtained at 200 °C and 0.01 s^{-1} exhibits distinctive softening after passing peak stress without steady-state flow.

In order to determine the material parameters according to Eq. 1, different plots of flow stresses against strain rates as well as reciprocal temperatures have to be carried out. More detailed information for the accurate estimation of the material constants is given in [6].

The slope obtained by plotting ln(strain rate) against lnsinh(α·peak stress) at varied temperatures and adjusting the stress multiplier α to make the plots at all temperatures parallel as possible delivers the temperature compensated strain rate sensitivity n. Figure 4 shows such plots for the high-temperature regime (400–500 °C) of AZ31 for the peak stress as well as the flow stress at a strain of 0.5 (steady-state). In both plots the strain rate sensitivity slightly decreases with the increasing temperature ranging from 4.83 to 4.4 (average value $n_{avg} = 4.5$) for the peak stress and respectively from 5.87 to 4.6 (average value $n_{avg} = 5.1$) for the steady-state stress. The plots of the other conditions processed in the same way give similar results and therefore are not presented here. In general, ME21 shows similar behavior yielding an average value of 4.7. At lower test temperatures (200–400 °C) AZ31 shows increasing strain rate sensitivity delivering increasing values. The average value for the peak stress was 6.3. Considering the flow stress at a strain of 0.5 AZ31 delivers a value of ~5.8.

The apparent activation energy Q for deformation can be estimated by transforming the Eq. 1 to

$$Q = R \cdot \left[\frac{\partial \ln \dot{\varepsilon}}{\partial \ln \sinh(\alpha\sigma)}\right]_T \cdot \left[\frac{\partial \ln \sinh(\alpha\sigma)}{\partial (1/T)}\right]_{\dot{\varepsilon}}. \quad (2)$$

The first term is already depicted in Fig. 4. By plotting lnsinh(α·stress) against 1,000 T^{-1} the second term of Eq. 2 can be diagramed. Figure 5 presents the plot of lnsinh(α·stress) for AZ31 as a function of the reciprocal temperature for the peak stress as well as steady-state stress. By multiplying the average slope of the second term with the average strain rate sensitivity and the gas constant the apparent activation energy can be calculated. The material constants for ME21 as well as AZ31 in a temperature range of 200–400 °C were determined in the same way. All constitutive parameters are displayed in Table 1.

In the high-temperature regime (400–550 °C) the calculated apparent activation energy Q is significantly higher than the activation energy of pure magnesium for volume self-diffusion (value: 135 $kJmol^{-1}$ [14]). Moreover, for the flow stresses at a strain of 0.5 the activation energy rises to 197 $kJmol^{-1}$. Bruni et al. [18] already published similar high values. Barnett [19] also presented results for apparent

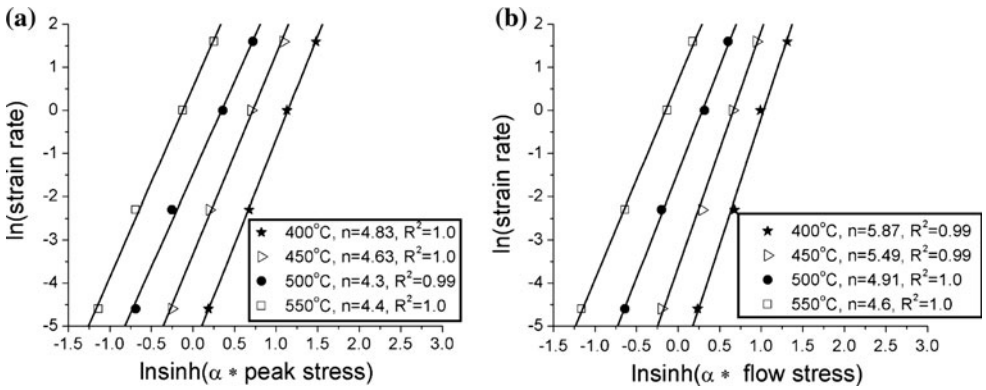

Fig. 4 **a** ln(strain rate) as a function of lnsinh(α·peak stress) and **b** ln(strain rate) as a function of lnsinh(α·flow stress) at a strain of 0.5 for AZ31

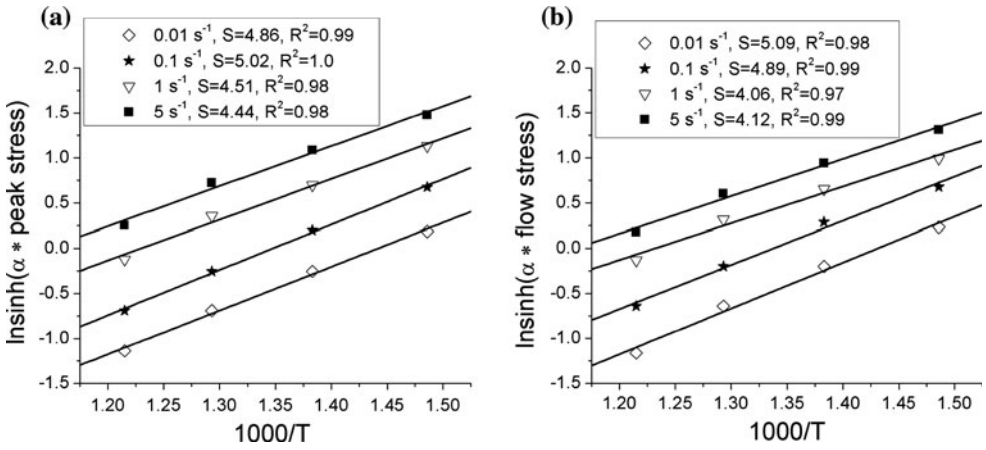

Fig. 5 **a** lnsinh(α·peak stress) as a function of 1,000 T^{-1} and **b** lnsinh(α·flow stress) at a strain of 0.5 as a function of 1,000 T^{-1}

Table 1 Constitutive parameters of AZ31 and ME21 for different temperature ranges as well as stress states

	T (°C)	Stress	Q (kJmol^{-1})	n_{avg}	A (s^{-1})	α (MPa^{-1})
AZ31	400–550	Peak	178	4.5	2.9E + 11	0.021
AZ31	400–550	Flow	197	5.1	6.4E + 12	0.022
AZ31	250–400	Peak	120	5.8	2.6E + 09	0.010
AZ31	250–400	Flow	108	6.3	4.9E + 08	0.010
ME21	400–550	Peak ≈ flow	182	4.7	3.5E + 11	0.023

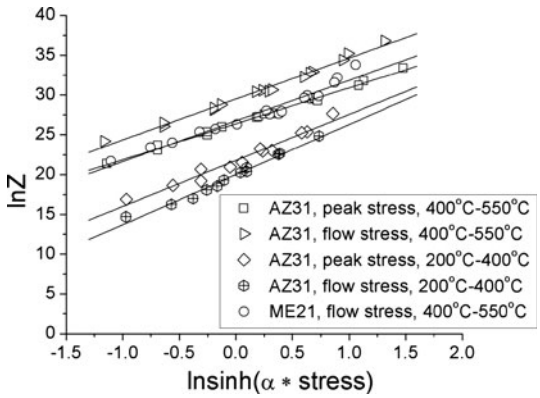

Fig. 6 LnZ as a function of lnsinh(α·stress) for different stress states and ranges of temperature

activation energy, which spans a wide range of values both higher and lower than the activation energy of self-diffusion and Wu and Liu [20] determined activation energy above 200 kJmol^{-1} in the high-strain rate regime. Furthermore, in [14] a value of 230 kJmol^{-1} for temperatures above 450 °C is published. Since the flow stresses of AZ31 and ME21 are not significantly different, the constitutive parameters of ME21 are close to that of AZ31. Thus, for the steady-state stress the apparent activation energy was approximately 182 kJmol^{-1}. Testing AZ31 in the lower range of temperatures (200–400 °C) the strain rate sensitivity increases close to six, whereas the apparent activation energy for deformation significantly decreases, delivering values of 120 kJmol^{-1} for the peak stress as well as 108 kJmol^{-1} for the flow stress. Therefore, the values of activation energy are between for that of grain boundary diffusion (value: 92 kJmol^{-1} [14]) and lattice diffusion. The results agree well with data presented in [14].

With the apparent activation energy the Zener–Hollomon parameter Z can be calculated according to Eq. 1. In Fig. 6 ln$Z$ is plotted as a function of lnsinh(α·stress) for different stress states and range of temperatures. Since the constitutive parameters of AZ31 and ME21 are very similar the Zener Hollomon parameters are close to each other. Due to the significantly lower activation energy at lower temperatures the values are distinctively smaller. Furthermore, the plot yields the values of the material parameter A, which is the intercept with the vertical axis.

In Fig. 7 the microstructures of deformed AZ31 at the strain of 0.5 are presented for different temperatures and strain rates. All deformed specimens showed highly heterogeneous deformation structures and partly recrystallized microstructures. The average size of new-formed DRX-grains as well as the fraction of DRX-grains increase with the increasing temperature and decreasing strain rate, i.e., decreasing Zener–Hollomon parameter, except for samples tested at 200 °C. The incomplete DRX found in all specimens after compression tests is attributed to the initial coarse grain size, which impedes the kinetics of DRX [21–23].

The microstructural evolution during deformation at 200 °C is contradictorily. Especially at very low-strain rates (0.01 s^{-1}) cracks and voids in the microstructure, which are mainly located in the vicinity of twins were found. With increasing strain rate less fractures occurred. Fractures along twin bands were often observed in samples exhibiting contraction twinning and double twinning (e.g., [24]). The observed strong flattening of the stress–strain curve is probably due to the occurrence of fracture, since

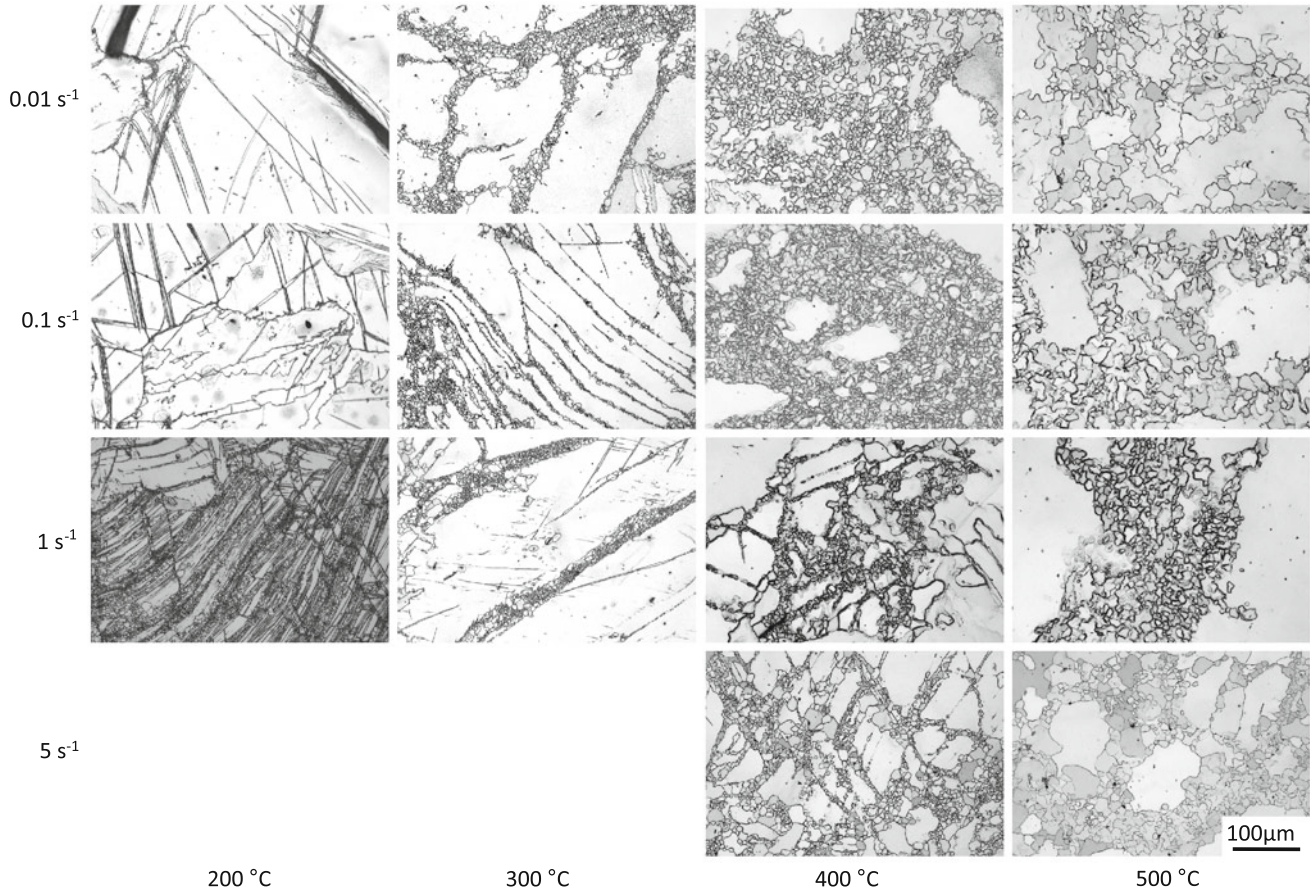

Fig. 7 Micrographs of deformed AZ31 dependending on temperature and strain rate at a strain of 0.5

no pronounced DRX could be observed. That is probably caused by the experimental setup. As already mentioned at higher strain rates the specimens adiabatically heated during deformation leading to increasing actual temperatures [15]. For instance, specimen deformed with a strain rate of 0.1 s^{-1} already delivered an increase in temperature of approximately 20 K, so that the actual deformation of the "200 °C-specimen" differed. This temperature difference increases with increasing strain rate. At 200 °C the apparent activation energy for deformation is very low resulting in a relatively high-deformation resistance. In addition, the temperature of 200 °C is the threshold, where non-basal slip systems can be temperature-activated (e.g., [1]). An increase in temperature drops down the CRRS and permits the activation of non-basal slip systems, leading to further available slip systems and finally in a more homogeneous plastic deformation. Furthermore, non-basal slip systems promote DRX by cross-slip and even climb [12]. Consequently, with increasing strain rate the fraction of DRX-grains increases.

Moreover, new-formed DRX-grains were found in many but not in all twins. Twins generally exhibit higher stored deformation energy than the un-twinned grains. Therefore, they are preferred to operate as nucleation sites for DRX-grains. Al-Samman and Gottstein [9] reported comparable findings identifying solely tensile twins, which permit nucleation of DRX-grains. In contrast, a recent investigation carried out by Yu and Choo [25] figured out a significant influence of contraction twins on grain refinement and even pointed out a transition of DRX processes from continuous DRX to twin-assisted DRX. At 300 °C (0.1, 1 s^{-1}) and even at 400 °C at high-strain rates (1, 5 s^{-1}), i.e., specimen showing a peak in stress–strain curve, DRX in twins was observed, whereupon the amount of twins decreases with decreasing strain rate and increasing temperature. However, fine necklace-type DRX-grains, which are formed by bulging of serrated grain boundaries and in shear bands, were found. With higher temperature the bulge of serrated grain boundaries for DRX nucleation predominates. Increasing temperatures deliver increasing apparent activation energies and therefore enhanced kinetics for DRX. Since the activation energy of plastic flow exceeds the energy for volume self-diffusion fast dislocation climb becomes the controlling process for plastic deformation and nucleation of DRX [12].

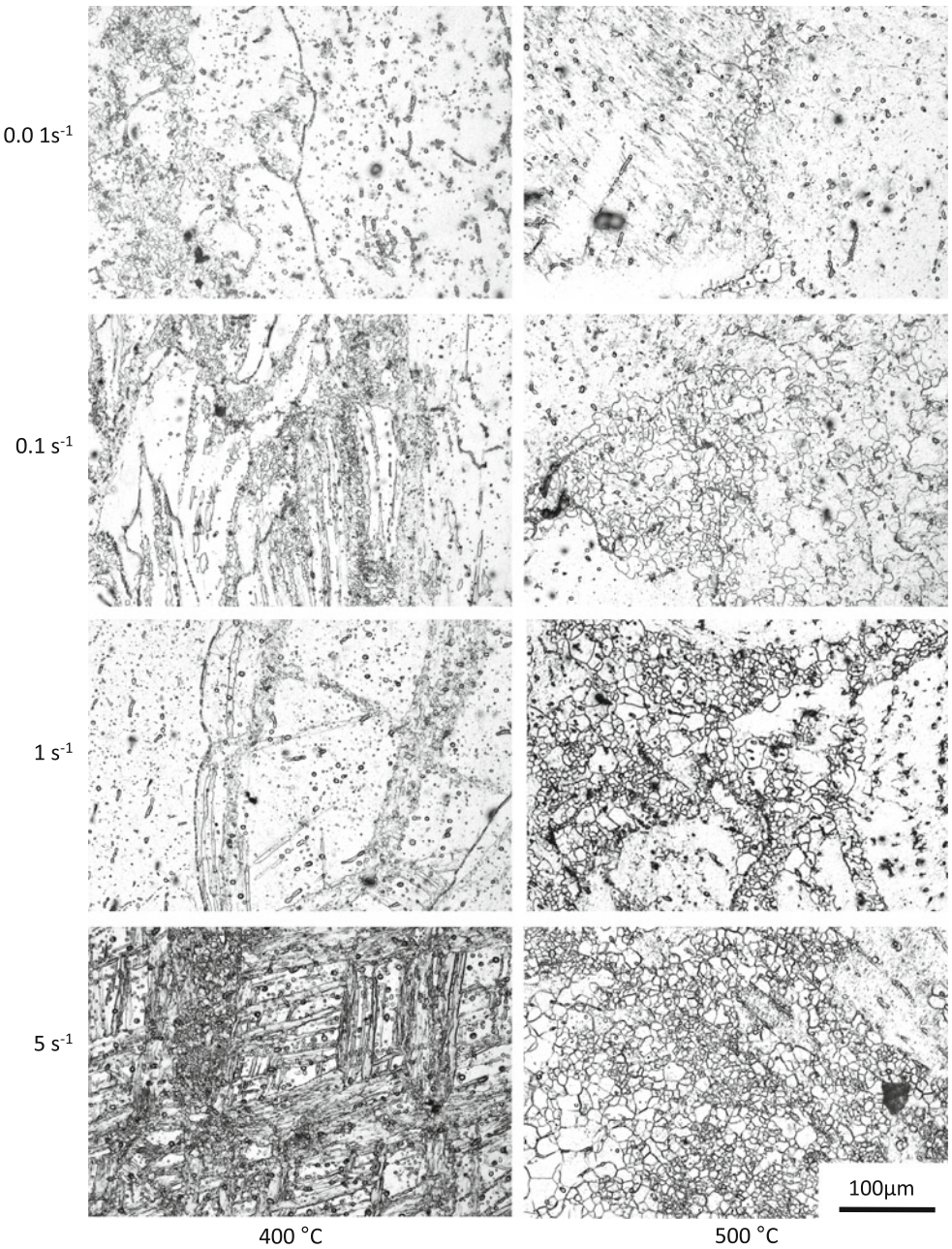

Fig. 8 Micrographs of deformed ME21 dependending on temperature and strain rate at a strain of 0.5

Even though the Zener–Hollomon parameter and the apparent activation for deformation of ME21 and AZ31 are very similar the microstructural evolution during the hot compression is significantly different. Figure 8 presents the micrographs of deformed ME21 for different deformation temperatures and strain rates. Again the deformed specimens are characterized by a heterogeneous structure and partly recrystallized microstructure, but compared to AZ31 the fraction of DRX-grains as well as the grain size is distinctly smaller. Grain nucleation predominantly occurs on bulging of serrated grain boundaries. DRX in twins and shear bands occurs, but not as pronounced as in AZ31. Furthermore, nucleation of grains in the vicinity of particles (particle-stimulated nucleation—PSN) is found. With increasing temperature and increasing strain rate an increasing content of DRX-grains is formed. Moreover, during hot compression voids were often observed, preferably at 400 °C and at low-strain rates. This is in conflict with results published by Chino et al. [26], which reported a more homogeneous deformation without formation of shear bands in Mg–Ce alloys resulting in the suppression of cracking, especially at low temperatures. It is evident that the suppression of DRX also constrains the formability. Due to lower content of twins and shear bands less nucleation sites for DRX are available. Indeed PSN is an additional active mechanism for nucleation of new grains,

but it strongly depends on the critical size of the particle [27, 28]. Investigations on Mg–Mn alloys carried out by Robson et al. [27] show that "PSN-grains" give a very small contribution to the overall volume fraction of recrystallization. Therefore, the dominant DRX mechanism in ME21 is attributed to bulging of serrated grain boundaries by dislocation climb. The poor DRX behavior at even very high temperature might be caused by the very fine manganese precipitations (seen in [16]) as well as stable $Mg_{12}Ce$ particle, which probably hinder the dislocation moving and hence the DRX.

Conclusions

The deformation behavior of the two magnesium alloys AZ31 and ME21 has been studied over a very wide range of temperatures and strain rates. The main conclusions are:

- The mechanical parameters of the two investigated magnesium alloys appeared to be quite similar in the high-temperature range. The determination of apparent activation energies for plastic deformation delivered values between 180 and 200 $kJmol^{-1}$, the strain rate sensitivity ranged between 4.5 and 5.1 for both alloys.
- At low-deformation temperatures AZ31 shows a strong strain rate sensitivity. However, lower activation energies are found, which are intermediate between the activation energies of grain boundary diffusion and lattice diffusion.
- The material parameter determined for peak stress and stresses at a strain of 0.5 (steady-state) differed not significantly.
- At 200 °C DRX was predominantly nucleated in twins. With increasing strain rate a rising amount of DRX-grains were visble, but with decreasing strain rate more voids and fracture in the vicinity of twins were found. It is assumed that this findings is caused by a more difficult formability at the real temperature of 200 °C compared with adiabatically heated samples.
- At higher temperature an increasing content of necklace-type DRX-grains were found. These grains are formed by bulging of serrated grain boundaries and in shear bands. At the high temperature range dislocation climb is recognized to control the processes responsible for nucleation of DRX and plastic deformation.
- In ME21 the onset of DRX is significantly diminished compared to AZ31. DRX in twins and shear bands occur, but not as distinctive as in AZ31. Besides particle-stimulated nucleation took place delivering only a small contribution to the total amount of DRX-grains. DRX predominantly occurred due to bulging of serrated grain boundaries.
- In ME21 the DRX is suppressed at an early stage of deformation due to the lower fraction of twins and shear bands, which are usually nucleation sites for DRX. Furthermore, it is supposed that dislocation movement is impeded by $Mg_{12}Ce$-particles and very fine manganese precipitates.

Acknowledgments The authors are grateful for the financial support from the Deutsche Forschungsgemeinschaft (DFG) under the contract number MU 2963/6-1. The assistance of Dirk Gräning (Metallic Materials, TU Berlin) during the compression tests and metallographic preparations is gratefully acknowledged.

References

1. Ion SE, Humphreys FJ, White SH (1982) Acta Metall 30:1909
2. Partridge PG (1967) Metall Rev 12:169
3. Meyers MA, Vöhringer O, Lubarda VA (2001) Acta Mater 49:4025
4. Barnett MR, Keshavarz Z, Beer AG, Atwell D (2004) Acta Mater 52:5093
5. Agnew SR, Duygulu Ö (2005) Int J Plast 21:1161
6. McQueen HJ, Ryan ND (2002) Mater Sci Eng A 322:43
7. Slooff FA, Zhou J, Duszczyk J, Katgerman L (2008) J Mater Sci 43:7165. doi:10.1007/s10853-008-3014-2
8. Slooff FA, Dzwonczyk JS, Zhou J, Duszczyk J, Katgerman L (2010) Mater Sci Eng A 527:735
9. Al-Samman T, Gottstein G (2008) Mater Sci Eng A 490:411
10. Poliak WI, Jonas JJ (1996) Acta Mater 44:127
11. Yin DL, Zhang KF, Wang GF, Han WB (2005) Mater Sci Eng A 392:320
12. Galiyev A, Kaibyshev R, Gottstein G (2001) Acta Mater 49:1199
13. Galiyev A, Kaibyshev R, Sakai T (2003) Mater Sci Forum 419–422:509
14. Frost HJ, Ashby MF (2012) The plasticity and creep of metals and ceramics version of deformation-mechanism maps. Cambridge University, Cambridge. http://engineering.dartmouth.edu/defmech/). Accessed 20 March 2012
15. Goetz RL, Semiatin SL (2001) J Mater Eng Perform 10:710
16. Huppmann M, Gall S, Müller S, Reimers W (2010) Mater Sci Eng A 528:342
17. Watanabe H, Tsutsui H, Mukai T, Kohzu M, Tanabe S, Higashi K (2001) Int J Plast 17:387
18. Bruni C, Donati L, El Mehtedi M, Simoncini M (2008) Key Eng Mater 367:87
19. Barnett MR (2001) J Light Met 1:167
20. Wu X, Liu Y (2002) Scripta Mater 46:269
21. Spigarelli S, El Mehtedi M, Cabibbo M, Evangelista E, Kaneko J, Jäger A, Gartnerova V (2007) Mater Sci Eng A 462:197
22. Hakamada M, Shimizu K, Yamashita T, Watazu A, Saito N, Iwasaki H (2010) J Mater Sci 45:719. doi:10.1007/s10853-009-3990-x
23. Figueiredo RB, Langdon TG (2010) J Mater Sci 45:4827. doi:10.1007/s10853-010-4589-y
24. Jain A, Duygulu O, Brown DW, Tomé CN, Agnew SR (2008) Mater Sci Eng A 486:545
25. Yu Z, Choo H (2011) Scripta Mater 64:434
26. Chino Y, Kado M, Mabuchi M (2008) Acta Mater 56:387
27. Robson JD, Henry DT, Davis B (2009) Acta Mater 57:2739
28. Shouren W, Ru M, Liying Y, Yong W, Yanjun W (2011) J Mater Sci 46:3060. doi:10.1007/s10853-010-5184-y